

<https://doi.org/10.15407/ujpe68.1.3>

N. KALZHIGITOV,<sup>1</sup> V.O. KURMANGALIYEVA,<sup>1</sup> N.ZH. TAKIBAYEV,<sup>1</sup>  
V.S. VASILEVSKY<sup>2</sup>

<sup>1</sup> Al-Farabi Kazakh National University  
(71 al-Farabi Ave., Almaty 050040, Kazakhstan;  
e-mails: knurto1@gmail.com, takibayev@gmail.com)

<sup>2</sup> Bogolyubov Institute for Theoretical Physics, Nat. Acad. of Sci. of Ukraine  
(14b, Metrolohichna Str., Kyiv 03143, Ukraine; e-mail: vsvasilevsky@gmail.com)

## RESONANCE STRUCTURE OF ${}^8\text{Be}$ WITHIN THE TWO-CLUSTER RESONATING GROUP METHOD

---

*A microscopic two-cluster model is applied to study the elastic alpha-alpha scattering and the resonance structure of  ${}^8\text{Be}$ . The model is an algebraic version of the Resonating Group Method (RGM), which involves the complete set of oscillator functions to expand the wave function of a two-cluster system. The interaction of nucleons inside each cluster and the interaction between clusters are determined by the well-known semirealistic nucleon-nucleon potentials which are employed in calculations. They differ by a size of the core at small distances between nucleons and realize the strong, moderate, and weak cores. They allow us to study dependence of calculated quantities on the shape of a nucleon-nucleon potential. The detailed analysis of resonance wave functions is carried out in the oscillator, coordinate, and momentum spaces. Effects of the Pauli principle on the wave functions of the  ${}^8\text{Be}$  continuous spectrum states are thoroughly studied.*

*Keywords:* cluster model, resonating group method, resonance states, Pauli principle.

### 1. Introduction

The nucleus  ${}^8\text{Be}$  is a very interesting object which attracts a large attention of various theoretical and experimental groups of researchers. This nucleus has no bound states, but it has a rich collection of resonance states. The low-energy part of resonance states belongs to the two-cluster continuum of two interacting alpha particles. There are three resonance states  $0^+$ ,  $2^+$ , and  $4^+$ , which are considered as a rota-

tional band of the  ${}^8\text{Be}$  nucleus. The  $0^+$  resonance state is a very narrow resonance state with the energy 0.092 MeV above the  $\alpha + \alpha$  decay threshold. The width of this state is 5.57 eV and the half-life time is  $8.19 \times 10^{-17}$  sec [1]. This allows one to treat it approximately as a bound state. Since the threshold energy of the second channel  $p + {}^7\text{Li}$  is 17.35 MeV with respect to the energy of the  $\alpha + \alpha$  channel, the  $\alpha + \alpha$  channel is dominant in a wide energy range ( $0 \leq E \leq 15$  MeV).

In the present paper, we are going to study the structure of  ${}^8\text{Be}$  and pay the main attention to the wave functions of resonance states. For this aim, we employ a specific version of the resonating group method (RGM) which was formulated in Refs. [2, 3] and is known as the algebraic version of the RGM. The key element of the algebraic ver-

Citation: Kalzhigitov N., Kurmangaliyeva V.O., Takibayev N.Zh., Vasilevsky V.S. Resonance structure of  ${}^8\text{Be}$  within the two-cluster resonating group method. *Ukr. J. Phys.* **68**, No. 1, 3 (2023). <https://doi.org/10.15407/ujpe68.1.3>.

Цитування: Калжігітов Н., Курмангалієва В.О., Такибаєв Н.Ж., Василевський В.С. Резонансна структура ядра  ${}^8\text{Be}$  у двокластерному методі резонуючих груп. *Укр. фіз. журн.* **68**, № 1, 3 (2023).

sion is that it uses the wave functions of a three-dimensional harmonic oscillator to expand the wave functions of an inter-cluster motion and realizes the matrix form of a quantum mechanical description of nuclear systems. The matrix form can be applied to study both bound and resonance states, since the corresponding boundary conditions, which are well known in the coordinate space, were transformed into a discrete oscillator representation. At the present time, the algebraic version of the resonating group method is a very efficient and popular tool to study the dynamics of two-cluster systems (Refs. [4–9]), and three-cluster systems as well (Refs. [10–13]).

The present paper is a continuation of the investigations of  ${}^8\text{Be}$  started in Ref. [7]. Note that the nucleus  ${}^8\text{Be}$  was a subject of the algebraic version of the resonating group method in Refs. [2, 14]. In the present paper, we will reveal a new interesting information on peculiarities of the dynamics of two-cluster systems and their manifestations in  ${}^8\text{Be}$ . We will discuss different ways of detecting resonance states and will show how resonance states affect the behavior of a lot of observable (partial and total cross-sections of elastic scattering and so on) and non-observable (wave functions, an average distance between clusters, and so on) physical quantities. As our model includes the oscillator basis, we will analyze the behavior of wave functions in the oscillator, coordinate, and momentum representations. An explicit evidence of a simple relation between the expansion coefficients and the corresponding wave function in the coordinate space will be shown for a continuous spectrum states.

The layout of the present paper is the following. In Sec. 2, we shortly review the principal ideas of the two-cluster model. In this section, we also introduce all necessary quantities which will be used to analyze the obtained results. Section 3 will start with the selection of nucleon-nucleon potentials with fixing all input parameters of our calculations. Then it proceeds with the analysis of the phase shifts of the elastic alpha-alpha scattering and the determination of the energies and widths of resonance states in  ${}^8\text{Be}$ . After that, peculiarities of the wave functions of resonance states and effects of the Pauli principle on continuous spectrum states of  ${}^8\text{Be}$  are discussed in detail. The final section summarizes main results of our investigations.

## 2. Method

Formulation of a microscopic method requires to display many-particle Hamiltonian and the explicit form of a wave function. The Hamiltonian which will be used in our calculations involves the kinetic energy operator, a semirealistic nucleon-nucleon potential, and the Coulomb interaction of protons. To achieve our goals, the sought wave function is selected to reproduce the two-cluster structure of  ${}^8\text{Be}$ . Therefore, the wave function of  ${}^8\text{Be}$  comprised of two alpha particles can be represented in the form

$$\Psi_{EL} = \hat{\mathcal{A}} \{ \Phi_1({}^4\text{He}, b) \Phi_2({}^4\text{He}, b) \psi_{EL}(q) Y_{LM}(\hat{\mathbf{q}}) \}, \quad (1)$$

where  $\hat{\mathcal{A}}$  is the antisymmetrization operator,  $\Phi_1({}^4\text{He}, b)$ , and  $\Phi_2({}^4\text{He}, b)$  are the translational invariant and antisymmetric functions describing the internal structure of the first and second alpha clusters, respectively. Since the spin of an alpha particle equals zero, the total spin  $S$  of  ${}^8\text{Be}$  equals also zero, and, therefore, the total angular momentum  $J$  coincides with the total orbital momentum  $L$ . Throughout of the text, we will use the total orbital momentum  $L$  to mark different rotation states of  ${}^8\text{Be}$ . A wave function  $\psi_{EL}(q)$  represents the radial motion of two clusters, while the spherical harmonic  $Y_{LM}(\hat{\mathbf{q}})$  represents the rotating motion of clusters. The Jacobi vector  $\mathbf{q} = q \cdot \hat{\mathbf{q}}$  ( $\hat{\mathbf{q}}$  is a unit vector whose orientation in space is fixed by two angles  $\theta_q$ , and  $\phi_q$ ) is proportional to the distance  $\mathbf{r}$  between interacting clusters

$$\begin{aligned} \mathbf{q} &= \mathbf{r} \sqrt{\frac{A_1 A_2}{A_1 + A_2}} = \\ &= \sqrt{\frac{A_1 A_2}{A_1 + A_2}} \left[ \frac{1}{A_1} \sum_{i \in A_1} \mathbf{r}_i - \frac{1}{A_2} \sum_{j \in A_2} \mathbf{r}_j \right], \end{aligned} \quad (2)$$

where  $\mathbf{r}_1, \mathbf{r}_2, \dots, \mathbf{r}_A$  are coordinates in the space of individual nucleons.

The main assumption of the RGM is that the wave functions  $\Phi_1({}^4\text{He}, b)$  and  $\Phi_2({}^4\text{He}, b)$  are known and fixed, while the intercluster function  $\psi_{EL}(q)$  has to be obtained by solving the dynamic equations. In the standard version of the RGM, one has to solve the integro-differential equation. The integral or nonlocal part of the equation appears due to the antisymmetrization operator or, in other words, due to the Pauli principle. In the algebraic version of the RGM, the dynamic equations transforms into a set

of linear algebraic equations. This is achieved by using a full set of the radial part of oscillator functions  $\{\Phi_{nL}(q, b)\}$ . By expanding the intercluster function  $\psi_{EL}(q)$  over oscillator functions

$$\psi_{EL}(q) = \sum_{n=0}^{\infty} C_{nL}^{(E)} \Phi_{nL}(q, b) \quad (3)$$

and the total two-cluster function  $\Psi_{EL}$  over cluster oscillator functions  $\{|nL\rangle\}$

$$\Psi_{EL} = \sum_{n=0}^{\infty} C_{nL}^{(E)} |nL\rangle, \quad (4)$$

we arrive to a system of linear algebraic equations

$$\sum_{\tilde{n}=0}^{\infty} \left\{ \langle nL | \hat{H} | \tilde{n}L \rangle - E \delta_{n\tilde{n}} \Lambda_{nL} \right\} C_{\tilde{n}L}^{(E)} = 0. \quad (5)$$

The cluster oscillator function  $|nL\rangle$  is determined as

$$\begin{aligned} |nL\rangle &= \\ &= \hat{\mathcal{A}} \{ \Phi_1({}^4\text{He}, b) \Phi_2({}^4\text{He}, b) \Phi_{nL}(q, b) Y_{LM}(\hat{\mathbf{q}}) \} \end{aligned} \quad (6)$$

We can see that the oscillator function  $\Phi_{nL}(q, b)$  describes the relative motion of two alpha particles in the cluster function (6), and takes the explicit form of the oscillator function

$$\Phi_{nL}(q, b) = \frac{(-1)^n}{b^{3/2}} \mathcal{N}_{nL} \rho^L e^{-\frac{1}{2}\rho^2} L_n^{L+1/2}(\rho^2), \quad (7)$$

$\rho = q/b.$

As we interested in the intercluster wave function in the momentum space  $\psi_{EL}(p)$ , we present also oscillator functions in the momentum space

$$\Phi_{nL}(p, b) = b^{3/2} \mathcal{N}_{nL} \rho^L e^{-\frac{1}{2}\rho^2} L_n^{L+1/2}(\rho^2), \quad (8)$$

$\rho = pb,$

where

$$\mathcal{N}_{nL} = \sqrt{\frac{2\Gamma(n+1)}{\Gamma(n+L+3/2)}},$$

and  $L_n^\alpha(z)$  is the generalized Laguerre polynomial [15].

The system of equations (5) contains matrix elements of the Hamiltonian between cluster oscillator functions  $\langle nL | \hat{H} | \tilde{n}L \rangle$  and matrix elements of the unit operator  $\langle nL | \tilde{n}L \rangle$ . For two-cluster systems, the matrix elements are diagonal with respect to quantum numbers  $n$  and  $\tilde{n}$  and coincide with the so-called eigenvalues of the norm kernel  $\Lambda_{nL}$

$$\langle nL | \tilde{n}L \rangle = \delta_{n,\tilde{n}} \Lambda_{nL}.$$

For  ${}^8\text{Be}$ , the eigenvalues  $\Lambda_{nL}$  equal

$$\Lambda_{nL} = \frac{1}{2} \sum_{k=0}^4 \frac{4! (-1)^k}{k! (4-k)!} \left[ 1 - k \frac{1}{2} \right]^{2n+L}. \quad (9)$$

The system of equations (5) is deduced directly from the Schrödinger equation

$$(\hat{H} - E) \Psi_{EL} = 0$$

for the wave function (1).

By solving the set of equations (5), we obtain the energy and a wave function of bound states or a wave function and the scattering  $S$ -matrix for continuous spectrum states. If, in Eq. (5), we restrict ourselves with a finite number (we denote it  $N$ ) of oscillator functions ( $n = 0, 1, \dots, N-1$ ), we encounter the generalized eigenvalue problem for  $N \times N$  matrices. By solving this problem, we obtain the energy spectrum  $E_\nu$  ( $\nu = 1, 2, \dots, N$ ) and wave functions  $\{C_{nL}^{(E_\nu)}\}$  of bound and pseudobound states. The latter are continuous spectrum states describing alpha-alpha scattering states under specific conditions. It was shown in Ref. [16] that the wave functions of pseudobound states in the oscillator space have a node at the point  $N$ , i.e.

$$C_{NL}^{(E_\nu)} = 0.$$

Thus, the diagonalization of the Hamiltonian with a fixed number of oscillator functions selects, from continuous spectrum states, those states which obey this specific boundary condition.

To solve the system of equations (1) for a scattering state, one has to formulate proper boundary conditions in the discrete oscillator space and then incorporate them in a set of equations (5). This problem has been numerously discussed in the literature (see, for instance Refs. [2, 3, 17, 18], [19]). Here, we shortly outline practical steps to obtain and analyze scattering states.

In the oscillator space like in the coordinate space, we split the space into two parts: internal and asymptotic regions. Let us recall how boundary conditions are formulated and used in the coordinate space. In the internal region, the interaction between clusters is prominent, and it should be treated correctly. In the asymptotic region, the interaction between clusters originates from a short-range nucleon-nucleon potential, is negligibly small, and can be ignored. As a consequence of this fact, the Hamiltonian in the asymptotic region consists of the kinetic energy operator  $\hat{T}_q$

of relative motion of clusters for neutral clusters (or when one of the clusters is a neutron). For charged clusters, it consists of the same kinetic energy operator and the Coulomb interaction of two point-like charged particles

$$\hat{H} = \hat{T}_q + \frac{Z_1 Z_2 e^2}{q} \sqrt{\mu}, \quad (10)$$

where  $Z_1(Z_2)$  is a charge of the first (second) cluster,  $e^2 = 1.44 \text{ MeV} \cdot \text{fm}$  is the square of the elementary charge in nuclear units, and

$$\hat{T}_q = -\frac{\hbar^2}{2m} \left[ \frac{d^2}{dq^2} + 2\frac{1}{q} \frac{d}{dq} - \frac{L(L+1)}{q^2} \right], \quad (11)$$

$$\mu = \frac{A_1 A_2}{A_1 + A_2}.$$

It is well-known (see, e.g., books [20, 21]) that Hamiltonian (10) leads to two independent solutions

$$\psi_{kL}^{(R)}(q) = \sqrt{\frac{2}{\pi}} k \frac{F_L(\rho, \eta)}{\rho}, \quad (12)$$

$$\psi_{kL}^{(I)}(q) = \sqrt{\frac{2}{\pi}} k \frac{G_L(\rho, \eta)}{\rho},$$

where  $\rho = kq$ ,  $\eta$  is the Sommerfeld parameter:

$$\eta = \frac{Z_1 Z_2 e^2}{\hbar k} \sqrt{\mu n}. \quad (13)$$

Wave functions  $\psi_{kL}^{(R)}(q)$  and  $\psi_{kL}^{(I)}(q)$  describe the scattering of charged particles and are regular and irregular (singular) at the origin of coordinates. For neutral particles, when  $\eta = 0$ , these functions are the spherical Bessel and Neumann functions

$$\psi_{kL}^{(R)}(q) = \sqrt{\frac{2}{\pi}} k j_L(\rho), \quad (14)$$

$$\psi_{kL}^{(I)}(q) = -\sqrt{\frac{2}{\pi}} k n_L(\rho, \eta),$$

The general solution for Hamiltonian (10) is the following combination of regular and irregular functions:

$$\psi_{kL}^{(a)}(q) = \psi_{kL}^{(R)}(q) + \tan \delta_L \psi_{kL}^{(I)}(q), \quad (15)$$

where  $\delta_L$  is a phase shift for the elastic cluster-cluster scattering. If we managed to calculate the phase shift  $\delta_L$ , then we immediately determine the two-cluster wave function in the semiinfinite range of distances  $R_i \leq q < \infty$ , where  $R_i$  indicates the intercluster distance which marks a border between the internal and

asymptotic regions. Equation (15) explicitly demonstrates boundary conditions for scattering states in a single-channel case. The asymptotic wave function  $\psi_{kL}^{(a)}(q)$  at the point  $q = R_i$  has to be matched with the internal wave function  $\psi_{kL}^{(i)}(q)$ . We assume that it is determined by the numerical solution of the Schrödinger equation in the interval of intercluster distances  $0 \leq q < R_i$ . The boundary conditions then are read as

$$\psi_{kL}^{(i)}(R_i) = \psi_{kL}^{(a)}(R_i), \quad (16)$$

$$\left. \frac{d}{dq} \psi_{kL}^{(i)}(q) \right|_{q=R_i} = \left. \frac{d}{dq} \psi_{kL}^{(a)}(q) \right|_{q=R_i}, \quad (17)$$

where the asymptotic and internal wave functions are matched and their first derivatives as well. These conditions guarantee that the intercluster wave function and its first derivative are continuous at the point  $q = R_i$ .

The same ideas were essentially used to formulate boundary conditions in the oscillator representations. Here, we present the shortest way of explanation, but not completely rigorous. For the sake of simplicity, we consider neutral clusters. As we pointed out above, the Hamiltonian in the asymptotic region consists of the kinetic energy operator. In the oscillator representation, this Hamiltonian has the tridiagonal form or a Jacobi matrix. Nonzero matrix elements  $\langle m, L | \hat{T}_q | n, L \rangle$  of the kinetic energy operator are

$$\langle m, L | \hat{T}_q | n, L \rangle = \frac{\hbar^2}{2mb^2} \times$$

$$\times \begin{cases} -\sqrt{n \left( n + L + \frac{1}{2} \right)}, & m = n - 1, \\ \left( 2n + L + \frac{3}{2} \right), & m = n, \\ -\sqrt{(n+1) \left( n + L + \frac{3}{2} \right)}, & m = n + 1. \end{cases} \quad (18)$$

It was shown in Refs. [18, 22, 23] that the matrix equation

$$\sum_{n=0}^{\infty} \left[ \langle m, L | \hat{T}_q | n, L \rangle - E \delta_{mn} \right] C_{nL} = 0 \quad (19)$$

has two independent solutions  $C_{nL}^{(R)}(kb)$  and  $C_{nL}^{(I)}(kb)$ . Traditionally, we refer to them as to regular and irregular solutions of Eqs. (19). The explicit form of

the solutions  $C_{nL}^{(R)}(kb)$  and  $C_{nL}^{(I)}(kb)$  can be found in Ref. [18, 22, 23]. It was shown in Refs. [2, 3] that, for large values of  $n$ , the expansion coefficients  $C_{nL}^{(R)}(kb)$  and  $C_{nL}^{(I)}(kb)$  are connected to the regular and irregular functions (14) by the simple relations

$$C_{nL}^{(R)}(kb) \approx \sqrt{2R_n} \psi_{kL}^{(R)}(R_n), \quad (20)$$

$$C_{nL}^{(I)}(kb) \approx \sqrt{2R_n} \psi_{kL}^{(I)}(R_n), \quad (21)$$

where

$$R_n = b\sqrt{4n + L + 3} \quad (22)$$

is the turning point of a classical harmonic oscillator. Relations (20) and (21) reflect general properties of oscillator functions. To this end, the relations similar to (20) and (21) are valid for any functions of a two-cluster system and corresponding expansion coefficients. It was explicitly demonstrated in Ref. [9] for the wave function of the  ${}^6\text{Li}$  ground state. It was shown that the relation between the wave function and the expansion coefficients (20) and (21) is valid even for small values of  $n$  ( $n \geq 5$ ). In the present calculations, we use similar relations for the expansion coefficients of the asymptotic wave functions (12) for charged clusters.

To solve Eq. (5) for continuous spectrum states, we have to introduce appropriate the boundary conditions in that set of equations. For this aim, the infinite set of expansion coefficients is divided into two subsets – internal and asymptotic ones:

$$\begin{aligned} \{C_{nL}^{(E)}\} &= \\ &= \{C_{0L}^{(E)}, C_{1L}^{(E)}, \dots, C_{N-1L}^{(E)}, C_{\nu L}^{(R)} + \tan \delta_L C_{\nu L}^{(I)}\}, \quad (23) \end{aligned}$$

where index  $\nu$  ( $N \leq \nu < \infty$ ) numerates expansion coefficients in the asymptotic region. With such form of expansion coefficients, we have got  $N + 1$  unknown quantities ( $N$  expansion coefficients in the internal region and phase shift  $\delta_L$ ) to be determined. By substituting the expansion coefficients (23) in Eq. (5), we obtain

$$\begin{aligned} &\sum_{\tilde{n}=0}^{N-1} \{ \langle nL | \hat{H} | \tilde{n}L \rangle - E \langle nL | \tilde{n}L \rangle \} C_{nL}^{(E)} + \\ &+ \tan \delta_L \sum_{\nu \geq N} \langle nL | \hat{H} | \nu L \rangle C_{\nu L}^{(I)} = \\ &= - \sum_{\nu \geq N} \langle nL | \hat{H} | \nu L \rangle C_{\nu L}^{(R)}. \quad (24) \end{aligned}$$

It is important to underline that, in this system of equations, index  $n$  runs from 0 to  $N - 1$ , and, thus, we have a set of  $N + 1$  linear algebraic equations for  $N + 1$  unknown quantities. With regard to Eq. (19), we get the set of equations (24)

$$\begin{aligned} &\sum_{\tilde{n}=0}^{N-1} \{ \langle nL | \hat{H} | \tilde{n}L \rangle - E \langle nL | \tilde{n}L \rangle \} C_{nL}^{(E)} + \\ &+ \tan \delta_L \sum_{\nu \geq N} \langle nL | \hat{V} | \nu L \rangle C_{\nu L}^{(I)} = \\ &= - \sum_{\nu \geq N} \langle nL | \hat{V} | \nu L \rangle C_{\nu L}^{(R)}. \quad (25) \end{aligned}$$

This is a basic set of equations which allows us to obtain a phase shift and the wave function of continuous spectrum states. The numerical solution of this set of equations is performed with a finite sum over indices  $\nu$ . In our calculations presented bellow, the sum involves 20 terms.

We will not also dwell on calculations of matrix elements of the kinetic and potential energy operators, since their explicit form and reliable methods of their calculations can be found in Ref. [19].

It is worth to note that the wave function  $\Psi_{EL}$  for a bound or pseudobound state is traditionally normalized to unity

$$\langle \Psi_{EL} | \Psi_{EL} \rangle = \sum_{n=0}^{\infty} |C_{nL}^{(E)}|^2 = 1.$$

However, the corresponding intercluster function is normalized as

$$\langle \psi_{EL} | \psi_{EL} \rangle = S_L. \quad (26)$$

In the oscillator representation, it can be represented as

$$S_L = \sum_{n=0}^{\infty} |C_{nL}^{(E)}|^2 / \lambda_n. \quad (27)$$

The quantity  $S_L$  is proportional to the spectroscopic factor  $SF_L$  (see its definition, for instance, in [24, 25] and [26], Chapter 9), which play an important role in the theory of nuclear reactions, when the Pauli principle is treated approximately [25]. The factor  $SF_L$  is used to determine amount of a certain (definite) clusterization in a wave function of the compound system. It is obvious from the definition of the spectroscopic factor (26), that it can be determined for bound state only, when the norms of the wave functions  $\Psi_{EL}$  and  $\psi_{EL}$  are finite.

### 2.1. Definition of basic quantities

Having calculated the wave function of the ground or resonance state in the oscillator representation  $C_{nL}^{(E)}$ , we can easily construct the intercluster wave functions in the coordinate and momentum representations

$$\psi_{EL}(q) = \sum_{n=0} C_{nL}^{(E)} \Phi_{nL}(q, b), \quad (28)$$

$$\psi_{EL}(p) = \sum_{n=0} C_{nL}^{(E)} \Phi_{nL}(p, b). \quad (29)$$

One can use these functions to obtain the additional information on bound and resonance states. We will employ the wave function in the coordinate space  $\psi_{EL}(q)$  to calculate the average distance between clusters  $A_c$ , which can be defined as

$$A_c = b \sqrt{\langle \psi_{EL}(q) | q^2 | \psi_{EL}(q) \rangle} / \mu, \quad (30)$$

where  $\mu = A_1 A_2 / A$  is the reduced mass for a selected clusterization. Similarly, we can also determine the average momentum  $P_c$  of relative motion of two clusters

$$P_c = b^{-1} \sqrt{\langle \psi_{EL}(p) | p^2 | \psi_{EL}(p) \rangle}. \quad (31)$$

The average momentum  $P_c$  is related to the average kinetic energy of two-cluster relative motion by the simple relation

$$T_c = \frac{\hbar^2}{2m} P_c^2.$$

By considering the continuous spectrum states, we will calculate and analyze the weight of the internal part of a wave function, which is defined as

$$W_L(E) = \sum_{n=0}^{N_i-1} |C_{nL}^{(E)}|^2. \quad (32)$$

This definition of a weight is equivalent to the following definition:

$$W_L(E) = \int_0^R dq q^2 |\psi_{EL}(q)|^2. \quad (33)$$

The radius of the internal region  $R$  can be determined in a self-consistent way as

$$R \approx b \sqrt{4N_i + 2L + 3}.$$

Let us evaluate the behavior of the function  $W_L(E)$  in a simple case where the function  $\psi_{EL}(q)$  describes a free motion of two clusters with the orbital momentum  $L = 0$ . Then the wave function  $\psi_E(q) = \psi_{E,L=0}(q)$  is

$$\psi_E(q) = \sqrt{\frac{2}{\pi}} \frac{\sin(kq)}{q},$$

and the weight  $W(E) = W_{L=0}(E)$  is equal to

$$W(E) = \int_0^R dq q^2 |\psi_E(q)|^2 = \frac{2}{\pi} \left[ \frac{1}{2} R - \frac{\sin(2kR)}{4k} \right],$$

where  $k$  is the wave number

$$k = \sqrt{\frac{2mE}{\hbar^2}}.$$

Thus, in a simple case, the weight  $W(E)$  has, as a function of the energy, an oscillatory behavior and is decreased with increasing the energy  $E$  or wave number  $k$ . It is worth to note that, for small values of  $E$ , we get

$$W(E) \approx \frac{2}{3\pi} R(kR)^2.$$

The weight  $W(E)$  is equal to zero at  $E = 0$  and slowly increases as a linear function of the energy. Such a behavior of weights as functions of the energy suggests that these functions have a maximum at a relatively small energy. We will see below that the weights  $W_L(E)$  of the internal part of scattering wave functions allow us to find the positions of resonance states and to evaluate their widths.

Within our method, the parameters of resonance states are obtained from the corresponding phase shifts by using the Breit–Wigner formula for a phase shift around a resonance state. It is assumed that the phase shift  $\delta$  in a vicinity of the resonance state consists of a background (potential) phase shift  $\delta_p$  and resonance phase shift  $\delta_R$

$$\delta = \delta_p + \delta_R,$$

where the resonance phase shift is determined by the Breit–Wigner formula

$$\delta_R = -\arctan \left( \frac{\Gamma}{E - E_r} \right).$$

We also assume that the first derivative of the background phase shift with respect to the energy is much smaller than the first derivative of the resonance phase shift with respect to the energy. Then, the energy and width of a resonance state can be determined from the following equations:

$$\left. \frac{d^2\delta(E)}{dE^2} \right|_{E=E_r} = 0, \quad \Gamma = 2 \left[ \left. \frac{d\delta(E)}{dE} \right|_{E=E_r} \right]^{-1}. \quad (34)$$

These relations allow us to determine more correctly the energy and width of a resonance state, especially in the case where the background phase shift is not small, and where the resonance state is wide.

### 3. Results and Discussion

Before the calculations, we need to select a nucleon-nucleon potential and to fix some parameters. To analyze the structure of  ${}^8\text{Be}$ , we selected three semirealistic nucleon-nucleon potentials which are very often used in many microscopical models of light atomic nuclei. They are the Volkov N2 potential (VP) [27], the Minnesota potential (MP) [28, 29], and modified Hasegawa–Nagata potential (MHNP) [30, 31]. These potentials provide a fairly good description of the nucleon-nucleon interactions in the states with different values of the two-nucleon spin  $S$  and isospin  $T$ . They also give the acceptable energy and size parameters of light nuclei described by a wave function of the many-particle shell model. The main difference of these nucleon-nucleon potentials, which are of importance for our investigations, is that the MHNP has the largest repulsive core at small distances between nucleons, the VP has the smallest repulsive core, and the MP represents the intermediate case.

Having selected the nucleon-nucleon potential, we determine some input parameters of the model. First of all, we have one free parameter in our calculation. It is the oscillator length  $b$ . It is natural to choose such value  $b$  which minimizes the binding energy of an alpha particle. We slightly adjusted the Majorana exchange parameter  $m$  in the VP and MHNP, as well as the exchange parameter  $u$  of the MP. The adjusted and original exchange parameters are shown in Table 1. The optimal value of the oscillator length  $b$  is also indicated in Table 1.

It is of interest to compare the cluster-cluster potential generated by the selected nucleon-nucleon potentials. Unfortunately, it is a difficult task, since

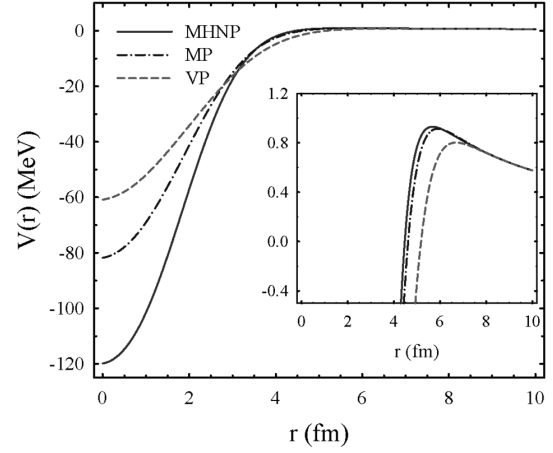


**Fig. 1.** Folding potential of the alpha-alpha interaction generated by the MHNP, MP, and VP

the cluster-cluster potential is a nonlocal energy-dependent interaction. This is due to the Pauli principle. However, we can compare the so-called folding potential, which is local and represents the main part of the cluster-cluster interaction, when the antisymmetrization between clusters is disregarded. This means that, in Eq. (1), the antisymmetrization operator  $\hat{A}$  is set to be  $\hat{A} = 1$ . In Fig. 1, the folding potentials generated by three nucleon-nucleon potentials are shown as a function of the intercluster distance. The folding potentials, like nucleon-nucleon potentials, have the Gaussian shape. However, contrary to the nucleon-nucleon potentials, the folding potentials have no repulsive core at small distances between alpha particles. As the folding potential involves the Coulomb interaction of protons, there is a barrier which stipulates the existence of the  $0^+$  resonance state. One can see that the MP and MHNP generate barriers of the same shape and height.

We start our investigations with the  $0^+$  phase shift of the elastic alpha-alpha scattering and the position of the  $0^+$  resonance state. In Fig. 2, we show the be-

**Table 1. Optimal values of oscillator length  $b$  and exchange parameter  $m$  or  $u$  of nucleon-nucleon potentials**

Potential	$b$ , fm	$m/u$ , adjusted	$m/u$ , original
VP	1.376	0.6011	0.600
MP	1.285	0.9347	–
MHNP	1.317	0.3961	0.4057

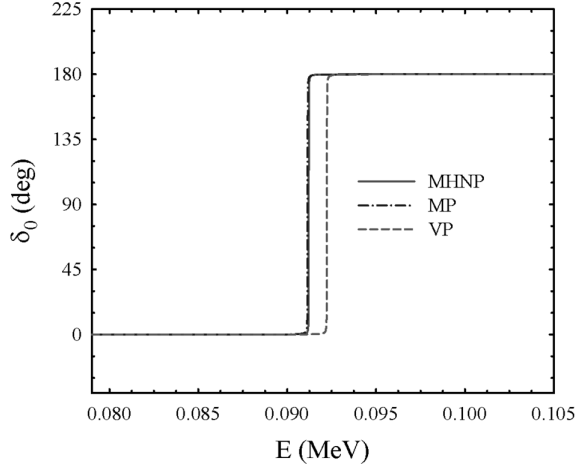


**Fig. 2.** Phase shifts of the alpha-alpha scattering with the zero value of the total orbital momentum

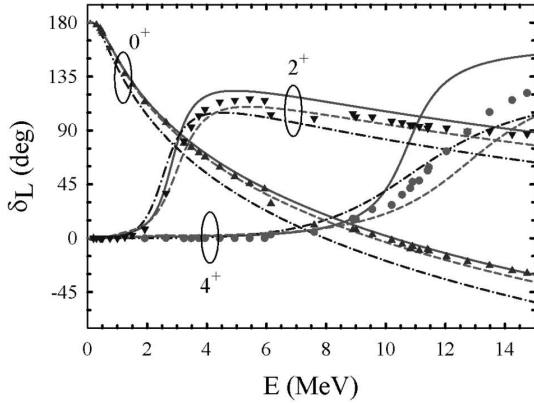


**Fig. 3.** Phase shifts of the elastic  $\alpha + \alpha$  scattering calculated with three different NN potentials and compared with experimental data. Notations are the same as in Fig. 2

havior of the  $0^+$  phase shift around the  $0^+$  resonance state. As we can see, this is an example of the classical Breit–Wigner resonance state, since the phase shift is increased on  $180^\circ$  at the resonance energy, and the background phase shift equals zero before and after that energy.

We also calculated phase shifts of the elastic alpha-alpha scattering and determined the position of the  $2^+$  and  $4^+$  resonance states. In Fig. 3, we demonstrate the dependence of phase shifts for the alpha-alpha elastic scattering on the energy and the shape of nucleon-nucleon potentials. The  $0^+$  phase shifts calculated with the MHNP and MP are very close in the whole range of energies displayed in Fig. 3. However, the  $0^+$  phase shifts calculated with VP are noticeably

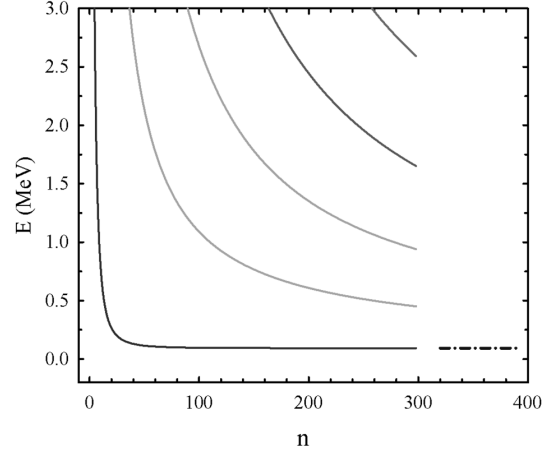


**Fig. 4.** Energy of the  $0^+$  states of  $^8\text{Be}$  as a function of the number of oscillator functions. Dash-dotted line indicates the position of the  $0^+$  resonance state. Results are obtained with the MHNP

different, despite that the VP, as the MHNP and MP, gives the correct position of the  $0^+$  resonance state, as it was demonstrated in Table 2. The difference between phases shifts of  $\alpha - \alpha$  scattering generated by three potentials is growing the total orbital momentum  $L$ . The difference is also reflected on the energy and width of the  $2^+$  and  $4^+$  resonance states (see Table 2).

Figure 3 demonstrates that there is a fairly good agreement of our results and experimental data. The experimental data displayed in Fig. 3 are taken from Refs. [32–35]. One can see that the MHNP and MP potentials yield the  $0^+$  and  $2^+$  phase shifts which are very close for experimental data in the presented range of energy. As for the phase shifts with the total orbital momentum  $4^+$ , our results are close to the experimental data at the energy range  $0 \leq E \leq 10$  MeV, and there is a deviation from experimental data for all potentials for the energy  $E > 10$  MeV.

### 3.1. Spectrum of resonance states

In Table 2, we compare the results of our calculations with the available experimental data [1]. The energy of resonance states is determined with respect to the  $\alpha + \alpha$  threshold energy.

There is another way to detect resonance states with a small width (i.e., narrow resonance states). This can be done by considering the spectrum of the two-cluster Hamiltonian as a function of the number



Table 2. Spectrum of resonance states in  ${}^8\text{Be}$ , calculated with three different nucleon-nucleon potentials and compared with experimental data

$L^\pi$	Potential	Theory		Experiment	
		$E$ , MeV	$\Gamma$ , MeV	$E$ , MeV	$\Gamma$ , MeV
$0^+$	MHNP	0.091	$5.183 \times 10^{-6}$	0.092	$(5.57 \pm 0.25) \times 10^{-6}$
	VP	0.091	$6.947 \times 10^{-6}$		
	MP	0.092	$5.876 \times 10^{-6}$		
$2^+$	MHNP	2.818	1.122	$3.122 \pm 0.010$	$1.513 \pm 0.015$
	VP	2.526	1.494		
	MP	2.977	1.773		
$4^+$	MHNP	10.633	1.816	$11.442 \pm 0.150$	3.500
	VP	10.852	6.732		
	MP	12.710	5.281		

of oscillator functions involved in calculations. Such dependence is shown in Figs. 4 and 5, where the spectra of  $0^+$  and  $2^+$  state are displayed. By a dash-dotted lines, we indicate the position of the  $0^+$  and  $2^+$  resonance states, calculated by using the corresponding phase shifts and Eqs. (34). As we see in Fig. 4, the energy of the lowest  $0^+$  state has a plateau exactly at the energy of the  $0^+$  resonance state. There is no plateau in Fig. 5 for the wide  $2^+$  resonance state. There are only small irregularities in the behavior of the energy of  $2^+$  states as a function of the number of oscillator functions  $N$ . Consequently, such type of fig-

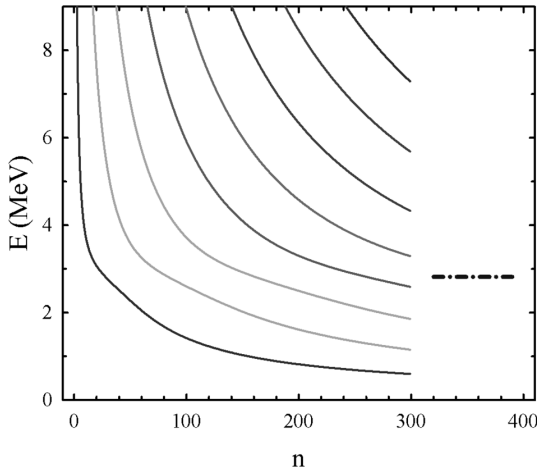


Fig. 5. Energy of  $2^+$  states of  ${}^8\text{Be}$  as a function of the number of oscillator functions. Dash-dotted line indicates the position of the  $2^+$  resonance state. Results are obtained with the MHNP

ures similar to Fig. 4 allows one to make predictions with a very good precision for the energy of a very narrow resonance state. This phenomenon is used in the Stabilization Method (see the formulation of this method in Ref. [36] and in some additional applications of the method [19]) to locate the position of resonance states.

The weights  $W(E)$  for the internal part of the scattering wave function introduced in Eq. (33) also reflect the existence of resonance states. We demonstrate it for the  $2^+$  states. The weights displayed in Fig. 6 are calculated with the MHNP (solid line)

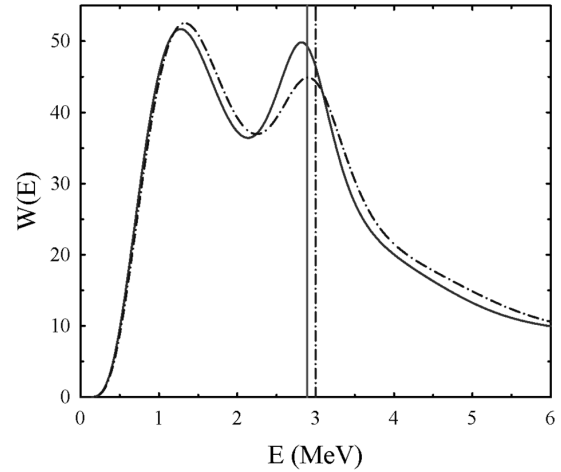
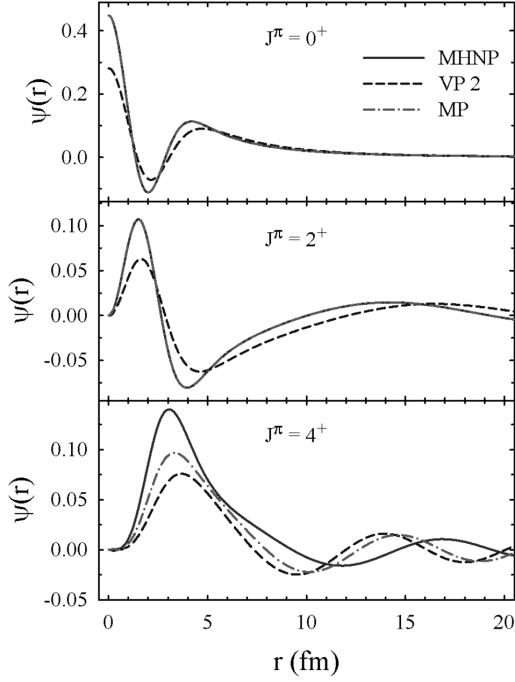
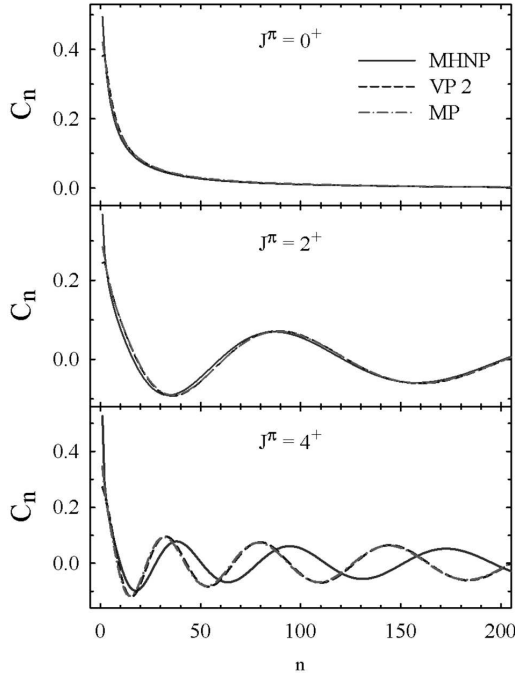


Fig. 6. The weights of the internal part of a scattering wave function as a function of the energy constructed for the  $2^+$  state with the MHNP (solid line) and MP (dot-dashed line). Vertical lines indicate the position of the  $2^+$  resonance states



**Fig. 7.** Wave functions of the  $0^+$ ,  $2^+$  and  $4^+$  resonance states as functions of the distance between alpha particles, calculated with the MHNP, VP, and MP



**Fig. 8.** Wave functions of  $0^+$ ,  $2^+$  and  $4^+$  resonance states in  $^8\text{Be}$  in the oscillator representation

and with the MP (dot-dashed line). The solid vertical and dot-dashed lines indicate the position of the  $2^+$  resonance states for the MHNP and MP, respectively. There are two peaks in Fig. 6. The first peak is not related to a resonance state, while the second one is formed by a resonance state. The center of the second peak is very close to the energy of the  $2^+$  resonance state. This figure demonstrates that the weights  $W_{L=2}(E)$  as functions of the energy can confirm the existence of rather wide resonance states and indicate their positions.

### 3.2. Resonance wave functions

In this section, we consider the wave functions of resonance states in  $^8\text{Be}$ . These functions are presented in the oscillator, coordinate, and momentum representations. We start with the coordinate representation. The wave functions  $\psi_{EL}(r)$  of the  $0^+$ ,  $2^+$ , and  $4^+$  resonance states are displayed in Fig. 7. It is worth to note that the maximum of the intercluster wave function of the  $0^+$  resonance state is at  $r = 0$ . Thus, the Pauli principle allows two alpha particles to be at the same point of the coordinate space. Due to the centrifugal barrier, the wave functions of the  $2^+$  and  $4^+$  resonance states equal zero at  $r = 0$ . Another interesting feature of all resonance states is that they have a large amplitude of the wave function in the internal region ( $0 \leq r < 7$  fm) and small amplitudes of oscillations in the asymptotic region ( $r > 7$  fm). The presented results allow us to investigate the dependence of resonance wave functions on the shape of a nucleon-nucleon potential. As we can see in Fig. 7, the MHNP and MP give almost identical wave functions for the  $0^+$  and  $2^+$  resonance states, but slightly different wave functions for the very broad  $4^+$  resonance state. In addition, the amplitudes of resonance wave functions calculated with the MHNP and MP are larger than those obtained with the Volkov potential.

In Fig. 8, we present the wave functions of the  $0^+$ ,  $2^+$  and  $4^+$  resonance states in the oscillator representation. The wave functions of the narrow  $0^+$  resonance states look like the wave functions of bound states. Our results confirm the conclusion made in Ref. [4] that the wave functions of narrow resonance states in the coordinate or oscillator representation are similar to those of bound states. We can see that the oscillator functions with  $0 \leq n < 20$  dominate in wave functions of all observed resonance states, since the expansion coefficients  $C_n$  associated with these

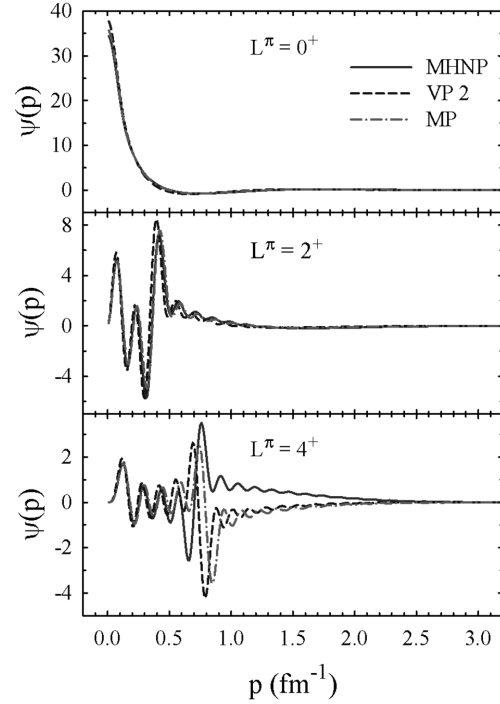
functions have the largest weight in resonance wave functions. The resonance wave functions in the oscillator representation are similar to the corresponding wave functions in the coordinate representation: they have large amplitudes in the internal region.

Figure 8 demonstrates that the wave functions of the  $0^+$  and  $2^+$  resonance states are almost independent of the shape of a nucleon-nucleon potential. The main difference between the wave functions for different nucleon-nucleon potentials is observed for the expansion coefficients with very small values of  $n$ . As for the wave function of the  $4^+$  resonance state, it is very close to those for the VP and MP, while the wave functions of the resonance states obtained with the MHNP are quite different.

The analysis of results presented in Figs. 7 and 8, shows that the larger the energy of a resonance state, the higher the number of oscillations of a resonance wave function in the coordinate and oscillator representations within the displayed range of the variables  $r$  and  $n$ , respectively.

The wave functions of resonance states in  ${}^8\text{Be}$  are also presented in the momentum space (Fig. 9). Figure 9 demonstrates that the wave functions of  $0^+$  and  $2^+$  resonance states are almost independent of the shape of a nucleon-nucleon potential. These wave functions are located in a very restricted region of the momentum  $p$ . The wave functions of the  $4^+$  resonance states obtained with different nucleon-nucleon potentials are quite different and spread in a more wider region of  $p$ . However, they are similar in the range of small values of the momentum:  $0 \leq p \leq 0.5 \text{ fm}^{-1}$ .

To demonstrate that our method is consistent with other alternative methods, we compare our results with those within the Complex Scaling Method (CSM) (its main ideas and recent achievements can be found in Ref. [37]) which allows one to determine a pole of the  $S$ -matrix and, consequently, the energy and width of resonance states directly from calculations of eigenvalues of the non-Hermitian Hamiltonian. Both calculations are performed for the MHNP and with the same input parameters. The results of these calculations are gathered in Table 3. It is seen that the results of our calculations are quite comparable with those of the CSM. The best agreement between two methods is achieved for the  $2^+$  and  $4^+$  resonance states, meanwhile the energy and width of the  $0^+$  resonance state are surprisingly different within these methods.



**Fig. 9.** Wave functions of the  $0^+$ ,  $2^+$  and  $4^+$  resonance states in  ${}^8\text{Be}$  in the momentum space. Results are presented for three NN potentials

It is well known that the Pauli principle plays the significant role in many-body fermion systems and particularly in many-cluster systems. The effects of the Pauli principle have been discussed in the literature from different points of view. We present another way of discussing the effect of the Pauli principle on the wave functions of continuous spectrum states in  ${}^8\text{Be}$ . We calculate and analyze the quantity  $S_L$  introduced in Eq. (27). This quantity is equal to unity, if the Pauli is disregarded or if its effects are negligibly small. Thus, a deviation of  $S_L$  from unity shows how

**Table 3. Parameters of resonance states calculated within the Resonating Group Method and the Complex Scaling Method**

$J^\pi$	Our method		CSM	
	$E$ , MeV	$\Gamma$ , MeV	$E$ , MeV	$\Gamma$ , MeV
$0^+$	0.091	$5.183 \times 10^{-6}$	0.150	$35.68 \times 10^{-5}$
$2^+$	2.820	1.196	2.893	1.135
$4^+$	10.730	1.925	10.824	1.916

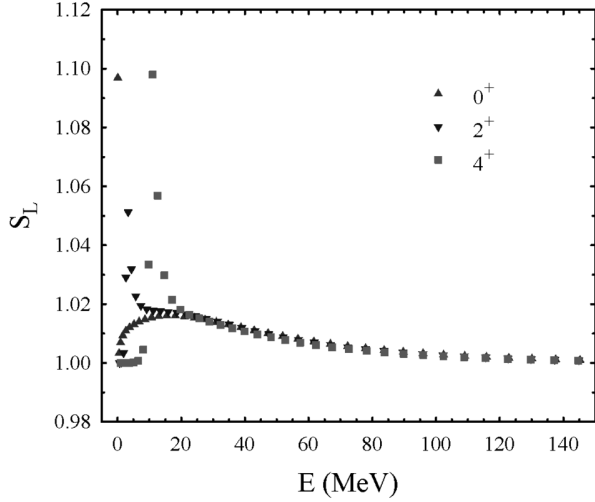


Fig. 10. Effects of the Pauli principle on the wave functions of  ${}^8\text{Be}$

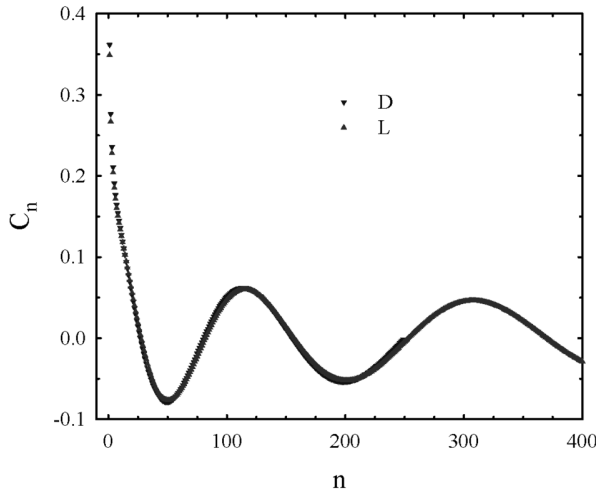


Fig. 11. Wave functions of the  $2^+$  state obtained with the diagonalization of the Hamiltonian ( $D$ ) and by solving the system of linear algebraic equations ( $L$ )

strong is the effect of the Pauli principle. In Fig. 10 we display  $S_L$  as a function of the energy for the  $0^+$ ,  $2^+$  and  $4^+$  states.

We see that the largest effect of the Pauli principle is observed for the eigenfunctions whose eigenvalues (eigenenergies) are very close to the energies of detected resonance states. This result reflects the main properties of resonance states, which are the most compact configurations among other states of the two-cluster continuum. The smaller the width of

a resonance state, the more compact is its configuration. Figure 10 shows that the low-energy states ( $0 \leq E \leq 50$  MeV) are more strongly affected by the Pauli principle than the states with large energies. With increasing the energy, the effects are gradually diminished. It is worth noting that the huge centrifugal barrier in the  $4^+$  state strongly diminishes the effects of the Pauli principle for the low-energy states ( $0 \leq E \leq 5$  MeV), where  $S_J \approx 1$ . The centrifugal barrier in the  $2^+$  state is approximately 3 times smaller than in the  $4^+$  state. Thus, the Pauli principle is stronger for the  $2^+$  state in this range of energy. It is worth to note that the results shown in Fig. 10 are in agreement with the conclusions made in Ref. [4], where two-cluster systems including  ${}^8\text{Be}$  have been studied in the Fock–Bargmann representations. This representation is a bridge between the quantum-mechanical treatment of nuclear systems and the classical one. In particular, it was shown that the classical regime is valid in the continuous spectrum of  ${}^8\text{Be}$ , when the energy of such states is larger than 60 MeV. Figure 10 also shows that the effects of the Pauli principle in this region are small.

To demonstrate the relation between the wave function obtained by the diagonalization of the Hamiltonian with a certain number of oscillator functions and a wave function calculated by solving the set of linear equations (5) with necessary boundary conditions, we used the following procedure. First, we diagonalize the  $250 \times 250$  matrix of the Hamiltonian for the  $2^+$  state and select an eigenstate with the energy close to that of the  $2^+$  resonance state. Thus, we selected the fourth eigenfunction with the energy  $E_4 = 2.929$  MeV. We denote this function as  $D$ , because it was obtained by the diagonalization. Second, we solved the system of linear algebraic equations with the energy very close to the energy of four eigenstates. We employ 400 oscillator functions to show the behavior of expansion coefficients in a large range of values of the index  $n$ . The wave function calculated in such way is marked as  $L$ . Since the functions are normalized in different ways, we renormalize the wave function  $L$  to make the comparison self-consistent. We divided the expansion coefficients  $\{C_{nL}^{(E)}\}$ , which represent the wave function  $L$ , by the square root of the sum  $S_{250}$

$$S_{250} = \sum_{n=0}^{249} |C_{nL}^{(E)}|^2.$$

Table 4. The mass root-mean-square radii and average distances between alpha particles for some pseudobound  $0^+$ ,  $2^+$  and  $4^+$  states

$L^\pi = 0^+$			$L^\pi = 2^+$			$L^\pi = 4^+$		
$E$ , MeV	$R_m$ , fm	$A_c$ , fm	$E$ , MeV	$R_m$ , fm	$A_c$ , fm	$E$ , MeV	$R_m$ , fm	$A_c$ , fm
0.091	3.11	6.35	0.610	11.31	22.62	6.44	9.67	19.35
0.462	10.74	21.48	1.168	10.14	20.28	8.07	9.44	18.88
0.953	10.01	20.02	1.876	9.49	18.99	9.71	8.62	17.25
1.664	9.89	19.78	2.624	8.25	16.51	11.03	7.59	15.24
2.604	9.84	19.69	3.329	8.32	16.67	12.60	8.93	17.87

As the result, a part of the wave function  $L$  represented with 250 oscillator functions is normalized in the same way as the wave function  $D$ . The renormalized wave function  $L$  and wave function  $D$  are demonstrated in Fig. 11. There is a small difference for the expansion coefficients with small values of  $n$ , which is due to a small difference of the energies of  $D$  and  $L$  states. In a large range of values of  $n$ , they are very close to each other. The wave function  $L$  can be easily expanded to very large values of  $n$  ( $n > 400$ ), since we know the asymptotic behavior of the function.

We select the wave function of  $2^+$  state, which is displayed in Fig. 11 and obtained from the diagonalization procedure, to show a relation between the coordinate wave function and expansion coefficients discussed above and presented in Eq. (20) and (21). Figure 12 visualizes such relation. We see that all expansion coefficients starting from  $n = 4$  are very close to those of the wave function in the coordinate space. This figure confirms once more that there is a simple relation between the coordinate and oscillator representations. This relation is valid not only for large values of index  $n$  as it was deduced originally, but also for fairly small values.

### 3.3. Average distances between clusters

In Table 4, we display the spectrum of  ${}^8\text{Be}$  obtained by diagonalizing the Hamiltonian, mass root-mean-square (rms) radii  $R_m$  of  ${}^8\text{Be}$  in these states, and the average distances  $A_c$  between clusters. These results are obtained with the MHNP. It is necessary to point out that the most compact configurations of  ${}^8\text{Be}$  are revealed in those eigenstates of the Hamiltonian whose energies are very close to the energy of resonance states. They are the first state for  $L^\pi = 0^+$

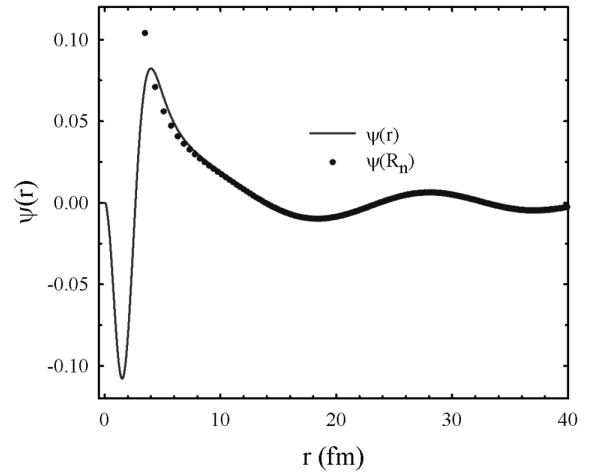
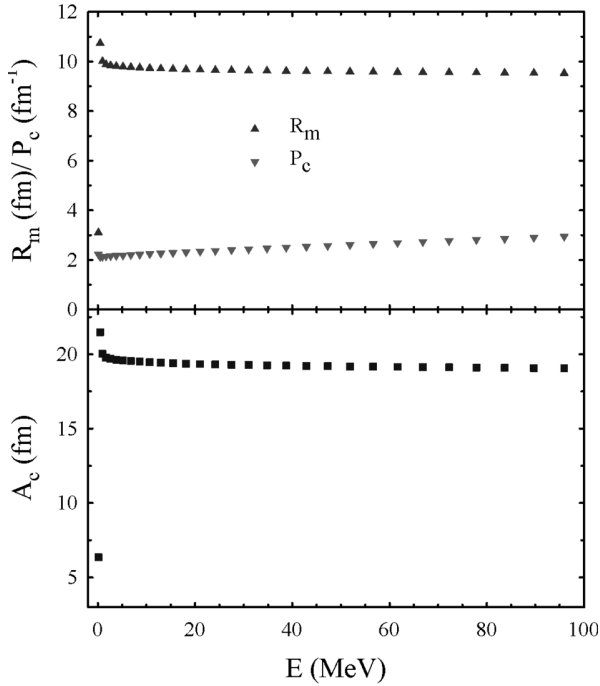


Fig. 12. Wave function  $\psi(r)$  of the  $2^+$  state with the energy  $E = 2.92$  MeV as a function of the intercluster distance (solid line) and expansion coefficients ( $\psi(R_n)$ ) as functions of the discrete distance  $R_n$

and the fourth state for  $L^\pi = 2^+$ . These two states have the smallest mass rms radius and smallest average distance between alpha particles. As is seen, the average distances are approximately two times larger than the corresponding mass rms radii. It is also worth noticing that the low-energy states (except the  $0^+$  resonance state) have the largest distance between alpha-particles. Thus, the low-energy states in the cluster model are very dispersed (stretched) states. This is stipulated by the shape of their wave functions which are dominantly represented by oscillator functions with large values of the index  $n$ .

In Table 4, we display five  $0^+$  and  $2^+$  states with the lowest energies, while, for the  $4^+$  states, we selected those eigenstates which are close by energy to the  $4^+$  resonance state. Results presented in Table



**Fig. 13.** The mass rms radius  $R_m$ , the average distance between alpha clusters  $A_c$ , and the average momentum of their relative motion  $P_c$  as functions of the energy obtained for the  $0^+$  states with the MHNP

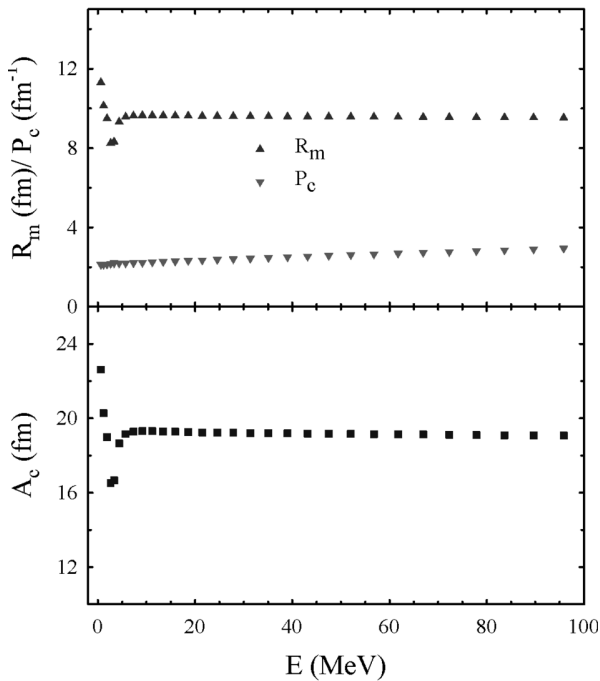


**Fig. 14.** The same as in Fig. 13 but for the states with  $J^\pi = 2^+$

4 show effects of the Pauli principle on a restricted set of eigenstates. The full picture of the effects for a large range of states is displayed in Figs. 13 and 14. In Fig. 13, we show, for the  $0^+$  states, the mass rms radii  $R_m$ , the average distance between alpha clusters  $A_c$ , and the average momentum  $P_c$  as functions of the energy. The same information is displayed in Fig. 14 for the  $0^+$  states.

The average distances between interacting clusters has been discussed in the literature in the case where cluster models are applied to study various nuclear hypernuclear systems. For example, in Refs. [38, 39], the hypernucleus  ${}^9_\Lambda\text{Be}$  has been studied within different threecluster models with the partition  $\alpha + \alpha + \Lambda$ . The nucleus  ${}^8\text{Be}$  comprised by two alpha particles is the major ingredient of the models. An approximate formula was used in Ref. [38] to extract the average  $\alpha - \alpha$  distance. Recall that we use a rigorous way for obtaining this quantity. The average distance between alpha particles was evaluated to be 5.99 fm in the ground  $0^+$  state which is close to our evaluation  $A_c = 6.35$  fm.

#### 4. Conclusions

We have applied a two-cluster microscopic model for the investigation of the alpha-alpha scattering and the resonance structure of  ${}^8\text{Be}$ . The model is the resonating group method with the matrix form of dynamic equations. The transition from the coordinate form to the matrix form is implemented with the help of oscillator functions. Three popular semirealistic nucleon-nucleon potentials are involved in calculations to determine both the internal energy of each cluster and the interaction between them. They also determine the dynamics of alpha-alpha scattering and the resonance structure of  ${}^8\text{Be}$ . These potentials are used to study the dependences of the spectrum, phase shifts, and wave functions of various states on the shape of a nucleon-nucleon potential. The slight tuning of parameters of the nucleon-nucleon potentials allowed us to reproduce, with a good accuracy, the energy and width of the  $0^+$  resonance state. The same parameters of the potentials are used to calculate  $0^+$ ,  $2^+$  and  $4^+$  phase shifts of elastic alpha-alpha scattering and the position of  $2^+$  and  $4^+$ . Our results are in a fairly good agreement with available experimental data and with results of other microscopical models.

It is shown that the Pauli principle has the largest impact on the wave functions of resonance states,

since the resonance states are the most compact two-cluster configurations among other states of the continuous spectrum. This is confirmed by calculations of the mass root-mean-square radius and average distance between alpha-particles. These calculations are performed with a large finite set of oscillator functions. It is also demonstrated that the effects of the Pauli principle are steadily decreasing with increasing the energy of  ${}^8\text{Be}$ .

*This work was supported in part by the Program of Fundamental Research of the Physics and Astronomy Department of the National Academy of Sciences of Ukraine (Project No. 0117U000239) and by the Science Committee of the Ministry of Education and Science of the Republic of Kazakhstan (Grant No. AP09259876).*

1. D.R. Tilley, J.H. Kelley, J.L. Godwin, D.J. Millener, J.E. Purcell, C.G. Sheu, H.R. Weller. Energy levels of light nuclei  $A = 8, 9, 10$ . *Nucl. Phys. A* **745**, 155 (2004).
2. G.F. Filippov, I.P. Okhrimenko. Use of an oscillator basis for solving continuum problems. *Sov. J. Nucl. Phys.* **32**, 480 (1981).
3. G.F. Filippov. On taking into account correct asymptotic behavior in oscillator-basis expansions. *Sov. J. Nucl. Phys.* **33**, 488 (1981).
4. Y.A. Lashko, G.F. Filippov, V.S. Vasilevsky. Dynamics of two-cluster systems in phase space. *Nucl. Phys. A* **941**, 121 (2015).
5. A.S. Solovyev, S.Y. Igashov, Y.M. Tchuvil'sky. Radiative Capture Processes in Multi-Size-Scale Algebraic Version of Resonating Group Model. *J. Phys. Conf. Ser.* **863**, 012015 (2017).
6. A.S. Solovyev, S.Y. Igashov, Y.M. Tchuvil'sky. Treatment of the mirror  ${}^3\text{H}(\alpha, \gamma)$   ${}^7\text{Li}$  and  ${}^3\text{He}(\alpha, \gamma)$   ${}^7\text{Be}$  reactions in the algebraic version of the resonating group model. *J. Phys. Conference Series* **569**, 012020 (2014).
7. V.S. Vasilevsky, K. Katō, V. Kurmangaliyeva, A.D. Duisenbay, N. Kalzhigitov, N. Takibayev. *Investigation of Discrete and Continuous Spectrum States in Two-Cluster System* (Hokkaido University, 2017).
8. A.D. Duisenbay, N.Zh. Takibayev, V.S. Vasilevsky, V.O. Kurmangaliyeva, E.M. Akzhigitova. Form factors and density distributions of protons and neutrons in  ${}^7\text{Li}$  and  ${}^7\text{Be}$ . *News Nat. Acad. Scien. Rep. Kazakhstan* **3** (325), 71 (2019).
9. N. Kalzhigitov, N.Z. Takibayev, V.S. Vasilevsky, E.M. Akzhigitova, V.O. Kurmangaliyeva. A microscopic two-cluster model of processes in  ${}^6\text{Li}$ . *News Nat. Acad. Scien. Rep. Kazakhstan: Phys.-Math. Ser.* **4** 332, (2020).
10. A.V. Nesterov, F. Arickx, J. Broeckhove, V.S. Vasilevsky. Three-cluster description of properties of light neutron and proton-rich nuclei in the framework of the algebraic version of the resonating group method. *Phys. Part. Nucl.* **41**, 716 (2010).
11. V.S. Vasilevsky, K. Katō, N. Takibayev. Systematic investigation of the hoyle-analog states in light nuclei. *Phys. Rev. C* **98**, 024325 (2018).
12. V.S. Vasilevsky, N. Takibayev, A.D. Duisenbay. Microscopic description of  ${}^8\text{Li}$  and  ${}^8\text{B}$  nuclei within three-cluster model. *Ukr. J. Phys.* **62** (6), 461 (2017).
13. A.D. Duisenbay, N. Kalzhigitov, K. Katō, V.O. Kurmangaliyeva, N. Takibayev, V.S. Vasilevsky. Effects of the Coulomb interaction on parameters of resonance states in mirror three-cluster nuclei. *Nucl. Phys. A* **996**, 121692 (2020).
14. I.P. Okhrimenko. Calculation of quasi-stationary state parameters within the algebraic version of the resonating-group method. *Few-Body Systems* **2**, 169 (1987).
15. M. Abramowitz, A. Stegun. *Handbook of Mathematical Functions* (Dover Publications, Inc., 1972).
16. G.F. Filippov, L.L. Chopovsky, V.S. Vasilevsky. On  ${}^7\text{Li}$  resonances in the  $\alpha + t$  channel. *Sov. J. Nucl. Phys. (Yad. Fiz.)* **37** (4), 839 (1983).
17. H.A. Yamani, L. Fishman,  $J$ -matrix method: Extensions to arbitrary angular momentum and to Coulomb scattering. *J. Math. Phys.* **16**, 410 (1975).
18. E.J. Heller, H.A. Yamani. New  $L^2$  approach to quantum scattering: Theory. *Phys. Rev. A* **9**, 1201 (1974).
19. G.F. Filippov, V.S. Vasilevsky, L.L. Chopovsky. Solution of problems in the microscopic theory of the nucleus using the technique of generalized coherent states. *Sov. J. Part. Nucl.* **16**, 153 (1985).
20. A.I. Baz, Ya.B. Zel'dovich, A.M. Perelomov. *Scattering, Reaction in Non-Relativistic Quantum Mechanics* (Israel Program for Scientific Translations, 1969).
21. R.G. Newton. *Scattering Theory of Waves and Particles* (McGraw-Hill, 1966).
22. H.A. Yamani, L. Fishman.  $J$ -matrix method: Extensions to arbitrary angular momentum and to Coulomb scattering. *J. Math. Phys.* **16**, 410 (1975).
23. Y.I. Nechaev, Y.F. Smirnov. Solution of the scattering problem in the oscillator representation. *Sov. J. Nucl. Phys.* **35**, 808 (1982).
24. M.H. Macfarlane, J.B. French. Stripping reactions and the structure of light and intermediate nuclei. *Rev. Mod. Phys.* **32**, 567 (1960).
25. N.K. Glendenning. *Direct Nuclear Reactions* (World Scientific, 1983).
26. O.F. Nemets, V.G. Neudachin, A.T. Rudchik, Yu.F. Smirnov, Yu.M. Tchuvil'sky. *Nucleon Clusters in Atomic Nuclei and Many-Nucleon Transfer Reactions* (Naukova Dumka, 1988), (in Russian).
27. A.B. Volkov. Equilibrium deformation calculation of the ground state energies of  $1p$  shell nuclei. *Nucl. Phys.* **74**, 33 (1965).
28. D.R. Thompson, M. LeMere, Y.C. Tang. Systematic investigation of scattering problems with the resonating-group method. *Nucl. Phys. A* **286** (1), 53 (1977).
29. I. Reichstein, Y.C. Tang. Study of  $N + \alpha$  system with the resonating-group method. *Nucl. Phys. A* **158**, 529 (1970).

30. A. Hasegawa, S. Nagata. Ground state of  ${}^6\text{Li}$ . *Prog. Theor. Phys.* **45**, 1786 (1971).
31. F. Tanabe, A. Tohsaki, R. Tamagaki.  $\alpha\alpha$  scattering at intermediate energies. *Prog. Theor. Phys.* **53**, 677 (1975).
32. N.P. Heydenburg, G.M. Temmer. Alpha-alpha scattering at low energies. *Phys. Rev.* **104**, 123 (1956).
33. T.A. Tombrello, L.S. Senhouse. Elastic scattering of alpha particles from helium. *Phys. Rev.* **129**, 2252 (1963).
34. P. Darriulat, G. Igo, H.G. Pugh, H.D. Holmgren. Elastic scattering of alpha particles by helium between 53 and 120 MeV. *Phys. Rev.* **137**, 315 (1965).
35. W.S. Chien, R.E. Brown. Study of the  $\alpha+\alpha$  system below 15 MeV (c.m.). *Phys. Rev. C* **10**, 1767 (1974).
36. A.U. Hazi, H.S. Taylor. Stabilization method of calculating resonance energies: Model problem. *Phys. Rev. A* **1**, 1109 (1970).
37. T. Myo, Y. Kikuchi, H. Masui, K. Katō. Recent development of complex scaling method for many-body resonances and continua in light nuclei. *Progr. Part. Nucl. Phys.* **79**, 1 (2014).
38. Y. Kanada-En'yo. Excitation energy shift and size difference of low-energy levels in p-shell  $\Lambda$  hypernuclei. *Phys. Rev. C* **97**, 024330 (2018).
39. A.V. Nesterov, Y.A. Lashko, V.S. Vasilevsky. Structure of the ground and excited states in  ${}^9_\Lambda\text{Be}$  nucleus. *Nucl. Phys. A* **1016**, 122325 (2021).

Received 23.01.23

*Н. Калжигитов, В.О. Курмангалиева,  
Н.Ж. Такіббаєв, В.С. Василевський*

#### РЕЗОНАНСНА СТРУКТУРА ЯДРА ${}^8\text{Be}$ У ДВОКЛАСТЕРНОМУ МЕТОДІ РЕЗОНУЮЧИХ ГРУП

Мікроскопічну двокластерну модель застосовано для вивчення пружного альфа-альфа розсіяння та резонансної структури ядра  ${}^8\text{Be}$ . Дана модель є алгебраїчною версією методу резонуючих груп, яка залучає повний базис осциляторних функцій для розкладу хвильових функцій двокластерної системи. Взаємодія нуклонів у кожному кластері, а також взаємодія між кластерами визначається відомими напівреалістичними нуклон-нуклонними потенціалами. У розрахунках використано три нуклон-нуклонних потенціали. Вони відрізняються розміром кору на малих відстанях між нуклонами і реалізують великий, помірний, або малий кор. Це дає можливість вивчати залежність розрахованих величин від форми нуклон-нуклонного потенціалу. Проведено детальний аналіз хвильових функцій резонансних станів у координатному, імпульсному та осциляторному просторах. Проаналізовано вплив принципу Паулі на хвильові функції неперервного спектра ядра  ${}^8\text{Be}$ .

*Ключові слова:* кластерна модель, метод резонуючих груп, резонансні стани, принцип Паулі.